



Design, Manufacturing and Evaluation of Grazing Incidence X-Ray Optics

Fuchang Zuo^{1(✉)}, Loulou Deng¹, Haili Zhang¹, Zhengxin Lv¹, and Yueming Li¹

¹Beijing Institute of Control Engineering, Beijing, China
zfch-2004@163.com

Abstract. On November 10, 2016, the pulsar navigation test satellite 01 (XPNAV-01) was launched in Jiuquan Satellite Launch Center, and has currently obtained a lot of observation data. At present, the payload has obtained a huge amount of observation data, and the flux, spectrum, and profile of the target observed are obtained as well. High consistency with the observation data by other missions such as RXTE is shown. The function and performance of China's first grazing incidence X-ray optics onboard XPNAV-01 was verified in-orbit.

The design of the X-ray optics was carried out according to the requirements of the mission to obtain parameters of each layer of mirror and relationship between adjacent mirrors, and four-layer optics was designed. Focusing analysis was then implemented to optimize the parameters and evaluate the performance of the optics. The mirrors were fabricated by electroformed Ni replication, and roughness and reflectivity were tested. The results show that the performance of mirror meets the requirements. Finally, the effective area of the optics was evaluated based on the in-orbit data to verify the design and fabrication, providing guidance and laying foundation for the development of X-ray optics with larger effective area and better angular resolution.

Keywords: Multilayer nested · Grazing incidence · Optics · Manufacturing and test · Performance evaluation

1 Introduction

Over the past decade, X-ray astronomy has been flourishing, in which focusing X-ray telescopes have had a very prominent role in astronomy, cosmology and in positioning astrophysics at the frontier of fundamental physics, as well as space climate detection, pulsar observation and pulsar navigation. The critical component of X-ray telescope is X-ray optics. Various types of X-ray optics have been developed and adopted, such as collimated type, coded aperture, normal incidence, lobster eye and grazing incidence. The collimated type, coded aperture and normal incidence have been gradually falling into disuse in recent years. The lobster eye is only suitable for monitoring the spatial X-ray burst source, and the background is relatively in a high level. Normal incidence

National Key R&D Program of China (No.: 2017YFB0503300).

© Springer Nature Switzerland AG 2020

H. P. Urbach, Q. Yu (eds.), *5th International Symposium of Space Optical Instruments and Applications*, Springer Proceedings in Physics 232,
https://doi.org/10.1007/978-3-030-27300-2_18

reflection optics and refraction optics cannot focus X-ray effectively. To realize X-ray focusing and increase the detection area, only the grazing incidence reflection optics can be selected. The grazing incidence focusing optics is widely used in observation of X-ray point source and pulsar navigation, with advantages of reducing background and improving SNR. It plays an irreplaceable role in the field of space X-ray observation and pulsar navigation, and has become one of core components of X-ray astronomy and pulsar navigation [1–3].

2 Requirements on Optics of Pulsar Navigation

In the 1970s, the Wolter-I grazing incidence optics was first verified on Einstein telescope. It was realized that not all applications require imaging with high angular resolution (<1 arcmin) since then [4]. The high angular resolution is extremely costly, which is usually realized through high-precision figure and high rigidity of thicker mirrors, so the mirror substrate is heavy and expensive to polish.

The NICER (Neutron Star Interior Composition Explorer) of NASA was launched in June 2017 on the Dragon Spacecraft and installed on the International Space Station. It integrates 56 single-reflection parabolic concentrators with an effective area of $1800 \text{ cm}^2@1.5 \text{ keV}$ [5], realizing detection sensitivity of $1\text{E}-5 \text{ ph/cm}^2/\text{s/keV}$. In November 2017, NICER carried out in-orbit verification of the pulsar autonomous navigation test, and the data converges to within 10 km within 8 h. Subsequently, ground navigation simulation test with 2 days of observation data shows that the position navigation accuracy can converge to within 5 km within 2 days, and the speed error converges to within 5 m/s. NICER demonstrates X-ray pulsar navigation in space for the first time.

China launched the Pulsar Navigation Test Satellite 01 (XPNAV-1) on November 10, 2016. The goal is to “see” soft X-ray pulsars in space for the first time in China, thus demonstrating the grazing incidence focusing detector system. One of the payloads of the XPNAV-1 is a grazing incidence focusing pulsar detector, which also adopts a single-reflection parabolic concentrator. The total effective area of the instrument is about $3.3 \text{ cm}^2@1.5 \text{ keV}$, and the sensitivity is in the level of $10^{-3} \text{ ph/cm}^2/\text{s}$. According to the in-orbit observation data, the profile of Crab pulsar was successfully recovered, and the effective area and energy resolution of the instrument were analyzed. The long-term observation was carried out to study the radiation characteristics of Crab pulsar, such as flow rate and spectrum and photon TOA characteristics. A pulsar navigation test was carried out based on in-orbit observation data and ground analysis, and the navigation accuracy of 30 km was demonstrated [6].

Therefore, for the astronomical field of observing X-ray photons and the pulsar navigation of detecting TOA of a large number of X-ray photons, it is necessary to lower the high angular resolution required for imaging to obtain higher sensitivity of the instrument. To this end, a single parabolic reflection scheme (concentrator) with a simpler structure and a larger area to mass ratio can be used. The in-orbit performance of NICER and XPNAV-1 indicates that the single-reflection grazing incidence focusing optics meets the needs of pulsar navigation and plays a central role in improving navigation accuracy.

In this chapter, the multilayer nested grazing incidence focusing optics of XPNAV-1 payload was designed and analyzed. The electroforming nickel replication was adopted to manufacture the mirror, and the roughness and reflectivity of the processed mirror were measured. Based on the in-orbit observation data, the effective area of the optics was evaluated, and the correctness of the design and processing method was verified, which can lay the foundation for the subsequent development of the large-area grazing incidence optics.

3 Design of the Optics

The optical path of a single-layer parabolic lens is shown in Fig. 1.

Figure 1 shows the reflection of three parallel X-rays incident in the x - y plane on the parabolic mirror. It can be seen from the figure that the three parallel X-rays change direction after reflection and converge to a point since the paraboloid has a focusing effect.

If the inner mirror is designed with the small end diameter as reference, the large end diameter of the inner mirror will be smaller than the small end diameter of the outer mirror, that is, part of the incident light passes directly without reflection through the space between the two layers. Through analysis, however, if the large end diameter of the inner layer of mirror is exactly equal to the small end diameter of the outer layer of mirror, the small end of the outer layer of mirror will block the light reflected by the outer mirror, making it unable to reach the focal plane, resulting in a larger invalid geometric collection area.

Therefore, the multilayer nested optics is designed on the principle that the inner mirror does not block the light reflected by the outer mirror. Assuming that the outermost lens is the first layer, in order to make the mirrors in all layers have the

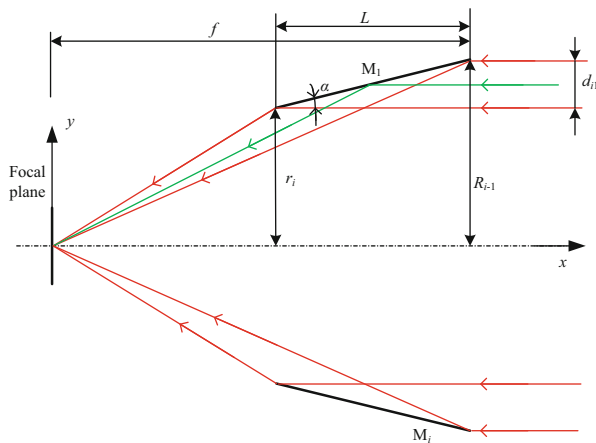


Fig. 1 Schematic diagram of optical path of a parabolic mirror

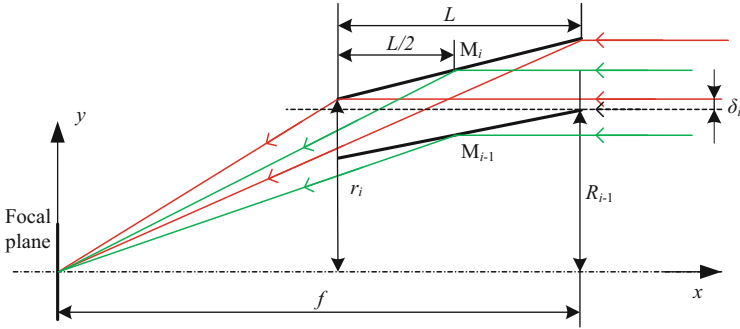


Fig. 2 Relationship between adjacent mirrors

same focal length, the space between the mirrors gradually decreases from outer to inner layers. The relationship between the mirrors is shown in Fig. 2:

The relevant parameters of layer 1 are:

Average grazing incidence angle: α_1 .

Focal length: f

Mirror length: L

Then the large end radius of the first layer mirror is:

$$R_1 = f \tan 2\alpha_1 + L \tan \alpha_1/2 \tag{1}$$

The small end radius is

$$r_1 = f \tan 2\alpha_1 - L \tan \alpha_1/2 \tag{2}$$

Based on the parameters of the first layer mirror, the parameters of inner layers are determined successively. The specific recursion formula is as follows:

$$r_{i+1} = r_i - L \tan 2\alpha_i + L \tan \alpha_i - t \tag{3}$$

$$\alpha_{i+1} = 2r_{i+1}/(4f - L) \tag{4}$$

$$R_{i+1} = r_{i+1} + L \tan \alpha_{i+1} \tag{5}$$

where $t = 0.5$ is the thickness of the mirrors.

For parallel incident X-rays, the effective area reduction per layer due to the presence of the gap between mirrors is approximately:

$$A_{\text{rec}} = \pi(R_{i-1} + t + r_i)d_i \tag{6}$$

The geometric collection area of each layer of lens is

$$A_i = \pi(R_i^2 - r_i^2) \tag{7}$$

Table 1 Parameters of the optics

Items	Values
Bandwidth	0.2–10 keV
FOV	$2\omega = 15'$
Focal length	1200 mm
Mirror length	140 mm
Mirror thickness	0.5 mm
Substrate material	Ni
Roughness	<0.5 nm (RMS)
Coating material	Iridium
On-axis effective area	15.6 cm ² @1 keV

Table 2 Parameters of mirrors

No. of mirror	Max radius R_{\max} (mm)	Min radius r_{\min} (mm)	Vertex radius of curvature r_0 (mm)	Grazing incidence angle α (rad)	Geometric area A_{geo} (mm ²)
1	50.00	46.99	1.0417	0.0208	916
2	46.36	43.58	0.8957	0.0193	788
3	42.95	40.37	0.7687	0.0179	676
4	39.75	37.36	0.6585	0.0166	579

The parameters of the four-layer nested grazing incidence optics are designed as shown in the following Tables 1 and 2:

4 Focusing Performance Analysis

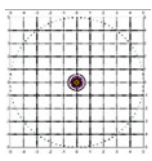
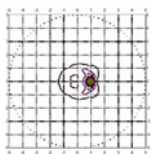
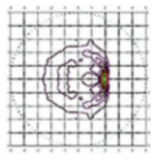
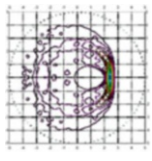
Taking the design parameters in Sect. 3 as input, the focusing performance of the optics designed was analysed. For the light incident at any angle within FOV, a spot is formed on the focal plane, but its size and the position of the centroid will change. The simulation results are shown in Table 3.

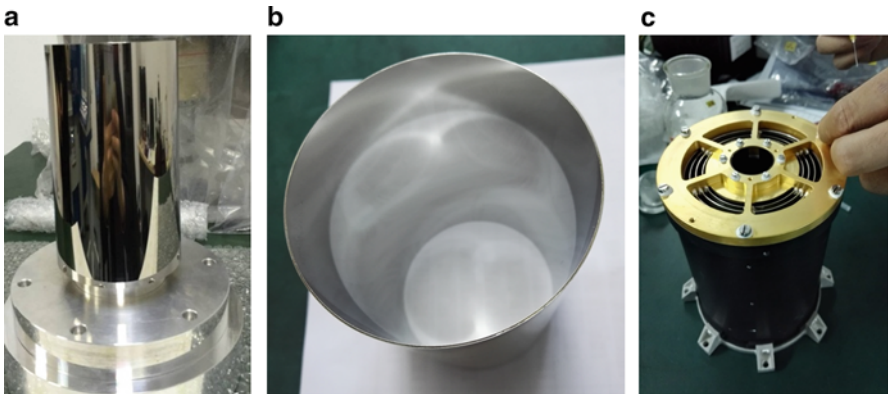
5 Manufacturing and Testing

Considering the advantages and disadvantages of several existing grazing incidence mirror manufacturing routes such as direct polishing, electroforming nickel replication, glass slumping replication, aluminium foils replication, and silicon micropore replication [7, 8], the electroforming nickel replication process similar to missions such as XMM and eRosita is adopted for the grazing incidence optics [9, 10]. The replication mandrel used for the outermost mirror and the replicated mirror are shown in Fig. 3.

The roughness of the mirror affects the X-ray reflectivity. The root mean square value σ of the roughness has the following relationship with the reflectivity R :

Table 3 Focusing performance at different incident angles

Incident angle	Scatter chart	Centroid (mm)
0°		0
0.05°		0.99
0.1°		1.96
0.125°		2.43

**Fig. 3** (a) Mandrel; (b) Mirror replicated; (c) Optics assembly

$$R(\theta) = \left| \frac{\sin \theta - \sqrt{\varepsilon - \cos^2 \theta}}{\sin \theta + \sqrt{\varepsilon - \cos^2 \theta}} \right|^2 \exp \left[-(4\pi\sigma \sin \theta / \lambda)^2 \right] \quad (8)$$

In order to improve the reflectivity, σ/λ must be as small as possible. For the designed energy bandwidth of 0.2–10 keV, the roughness must be smaller than 0.5 nm (RMS). The surface roughness of the polished mandrel was tested with the white light interferometer in the phase shift interference (PSI) mode. The result is shown in Fig. 4, and the surface roughness reaches 0.383 nm (RMS).

The reflectivity was tested at 4B7B beam line of the Beijing Synchrotron Radiation. The measured and theoretical calculation results are shown in Fig. 5.

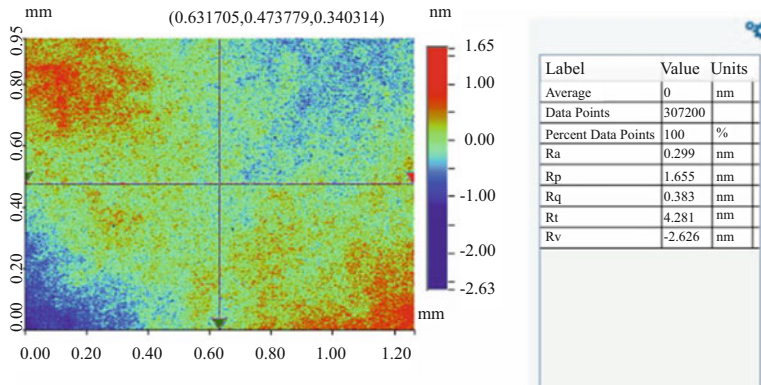


Fig. 4 Measured roughness

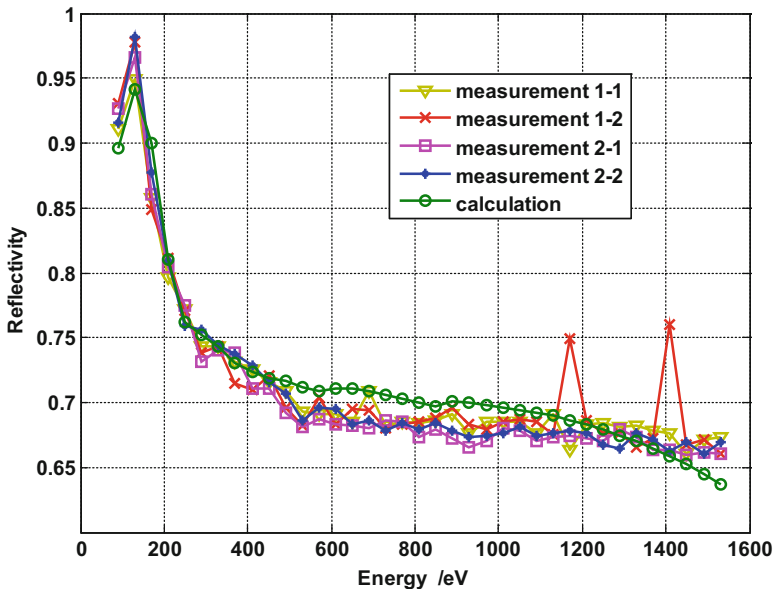


Fig. 5 Measured and calculated reflectivity

6 Performance Evaluation

Since the launch on November 10, 2016, the grazing incidence focused pulsar detector has obtained a large amount of observation data, through in-orbit data analysis, observation of target source characteristics analysis, and design parameters of the payload. The in-orbit effective area of the four-layer nested grazing incidence optics is evaluated.

6.1 Target Source Characteristics

The Crab Nebula soft X-ray band radiation is emitted from a sky area of approximately $100'' \times 100''$. The Crab Nebula soft X-ray band radiation consists of two parts: nebula background and Crab pulsar radiation.

The radiation flux of the Crab Nebula is consistent with the analytical formula of the following piecewise fit (unit: $\text{ph}/\text{cm}^2/\text{s}/\text{keV}$):

$$\begin{cases} I(E) = 20.7555 - 124.6E + 187E^2 & 0.3-0.5 \text{ keV} \\ I(E) = -13.925 + 38.59E - 19.5E^2 & 0.5-0.9 \text{ keV} \\ I(E) = 8.52853 - 4.65161E + 0.71452E^2 & 0.9-5.0 \text{ keV} \end{cases} \quad (9)$$

6.2 SDD Quantum Efficiency

The four-layer nested X-ray grazing incidence optics focuses the Crab pulsar X-ray photons onto a SDD detector, so the response curve of the SDD detector also affects the performance evaluation of the optics.

According to the manual of the SDD detector, the SDD quantum efficiency in the range of 0.2–5.0 keV is obtained by piecewise fitting as follows:

$$\begin{cases} \text{QE}(E) = -0.30125 + 1.34673E - 0.37946E^2 & 0.2-1.6 \text{ keV} \\ \text{QE}(E) = 0.19147 + 0.26572E - 0.02258E^2 & 1.6-5.0 \text{ keV} \end{cases} \quad (10)$$

6.3 Effective Area Evaluation

Thus, the efficiency of the optics in the range of 0.3–5.0 keV is

$$\eta_{\text{in-orbit}}(E) = \frac{F_{\text{observed}}(E)}{F_{\text{radiated}} \cdot \text{QE}(E)} = \frac{F_{\text{observed}}(E)}{I(E) \cdot \text{QE}(E) \cdot A_{\text{ap}}} \quad (11)$$

And the effective area is

$$A_{\text{eff}}(E) = \frac{F_{\text{obs}}(E)}{I(E) \cdot \text{QE}(E)} \quad (12)$$

According to the observation data F_{obs} , Crab pulsar target source characteristic (Eq. 9) and SDD detector response curve (Eq. 10), the effective area of the optics is evaluated as shown in Fig. 6.

It can be seen from Fig. 6 that the maximum effective area is $6.84 \text{ cm}^2 @ 0.7 \text{ keV}$, and the typical value is $4.22 \text{ cm}^2 @ 1 \text{ keV}$, which is lower than the design value of $15.6 \text{ cm}^2 @ 1 \text{ keV}$. We analyse that the reason for the smaller effective area is due to space thermal deformation and contamination of the optics in orbit. In the energy band of $0.3\text{--}0.7 \text{ keV}$, the effective area increases as the energy increases, and the trend is inconsistent with the theoretical calculation and ground test results. The reason for this is possibly that the Crab pulsar has a low flow intensity in the energy range of $0.3\text{--}0.7 \text{ keV}$, the randomness in X-ray photon energy is large, and the quantum efficiency of SDD in the energy range of $0.3\text{--}0.7 \text{ keV}$ is also low, causing the evaluation uncertainty to increase. In the energy range of $0.7\text{--}5 \text{ keV}$, the effective area trend is consistent with the ground test result, and the evaluation reliability is reliable.

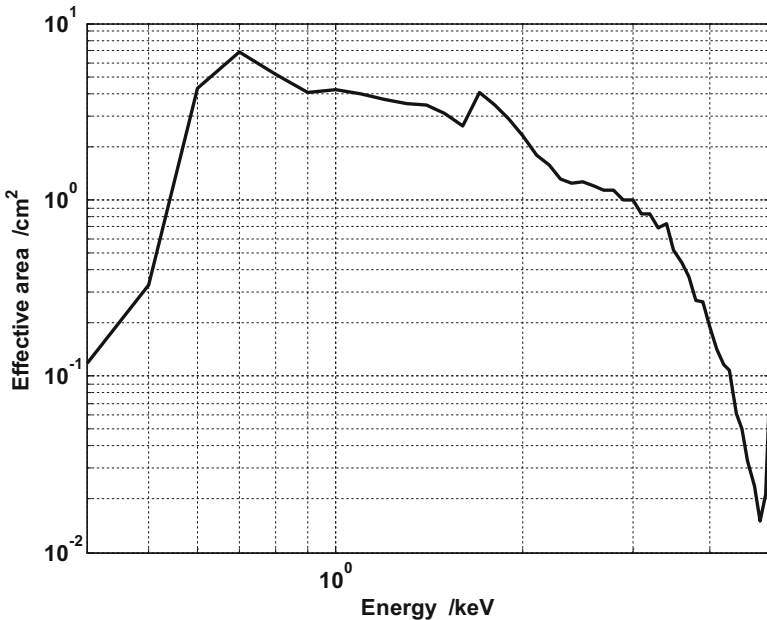


Fig. 6 Evaluated effective area based on in-orbit data

7 Conclusions

Through the optical design and derivation of the recursive relationship between each layer of mirrors of the multilayer nested grazing incidence optics, reasonable initial structural parameters of the optics are given. According to the initial structural parameters, optical analysis software is used to analyse the focusing performance. The electroforming Ni replication is adopted to manufacture the ultra-smooth mirror, and the measured roughness and reflectivity reached 0.383 nm and 67%@1.5 keV, respectively. According to in-orbit data analysis, observation target source characteristics analysis and design parameters of the optics, the effective area of the optics is evaluated to be 4.22 cm²@1 keV, which is much lower than the design value of 15.6 cm²@1 keV, which is caused by factors such as space environment and contamination during ground test, transport and storage.

This chapter provides guidance for the development of large-area multilayer nested X-ray grazing incidence optics. In addition to controlling the accuracy of the optics itself, it is also necessary to strengthen the control of environmental factors. At the same time, it is necessary to carry out space environment adaptability design and evaluation before launch.

References

1. Ray, P.S., Wood, K.S., Philips, B.F.: Spacecraft navigation using X-ray pulsars. *NRL Rev.* 95–102 (2006)
2. Emadzadeh, A., Speyer, J.L.: A new relative navigation system based on X-ray pulsar measurements. In: *IEEE Aerospace Conference, Big Sky, Montana*, pp. 1–8 (2010)
3. Gorenstein, P.: Focusing X-Ray Optics for Astronomy, vol. 2010, 19p. Hindawi Publishing Corporation X-Ray Optics and Instrumentation, Article ID 109740
4. Lorimer, D., Kramer, M.: *Handbook of Pulsar Astronomy*. Cambridge University Press, Cambridge, UK (2004)
5. Keith, C.G., Zaven, A., Takashi, O.: The neutron star interior composition ExploreR (NICER): an explorer mission of opportunity for soft x-ray timing spectroscopy. *Proc. SPIE.* **8443**, 8 (2012)
6. Lv, Z.X., Mei, Z.W., Deng, L.L., Li, L.S., Chen, J.W.: In-orbit calibration and dataanalysis of China's first grazing incidence focusing X-ray pulsartelescope. *Aerosp. China.* **18**(3), 3–10 (2017)
7. Petre, R.: Thin shell, segmented X-ray mirrors. *X-Ray Opt. Instrum.* **2010**, 15 (2010)
8. Louis, D., Robert, C., Takashi, O., Peter, S., Yang, S., Richard, K., et al.: Development of full shell foil X-ray mirrors. *Proc. SPIE.* **8450** (2012)
9. Friedrich, P., Bruninger, H., Budau, B., Burkert, W., Eder, J., Freyberg, M.J., et al.: Design and development of the eROSITA X-ray mirrors. *Proc. SPIE.* **7011**, 70112T-1–70112T-8 (2008)
10. Lumb, D.H., Schartel, N., Jansen, F.A.: X-ray multi-mirror mission (XMM-newton) observatory. *Opt. Eng.* **51**(1), 011009-1–011009-10 (2012)